SLAC-PUB-2620
October 1980
(E)

TIME-OF-FLIGHT MEASUREMENTS*

William B. Atwood
Stanford Linear Accelerator Center
Stanford University, Stanford, California 94305

Presented at the SLAC Summer Institute

Stanford, California

July 28 - August 8, 1980

*Work supported by the Department of Energy, contract DE-AC03-76SF00515.

I. INTRODUCTION

Time of flight (TOF) measurements are used in high energy particle physics experiments to: 1) distinguish background from events and 2) identify particle types. An example of background separation is shown Fig. 1.[1] These data come from a coincidence electro-production experiment performed at SLAC. The reaction being studied was $e + p \rightarrow e' + p' + X$ where the e(p) stand for an initial and detected electron (proton) and X is a produced but undetected final state with a mass in the ρ meson region. Plotted in Fig. 1 is the relative time between the detection of an electron and a proton in two of the spectrometers in End Station A. Data for two different kinematic settings taken in the experiment are shown. The time resolution has been partially corrected for the various flight paths through the instruments and the difference in time resolutions between the two settings results mainly from the incompleteness of this correction. The signal height above the background depends on the time resolution, $\Delta\tau$. The chance background is proportional to the product of the electron counting rate, the proton counting rate and $\Delta\tau$. Smaller $\Delta\tau$ means that higher electron and proton counting rates may be tolerated and result in a similar signal-to-noise ratio.

The second use of TOF measurements is to identify particle types. To utilize TOF measurements for particle identification requires that the momentum, p, of the particle also be measured. The time of flight difference for two particles of unequal mass is

$$\tau_1 - \tau_2 = \frac{\tau_o}{2}\left(\frac{M_1^2 - M_2^2}{p^2}\right) \qquad (1)$$

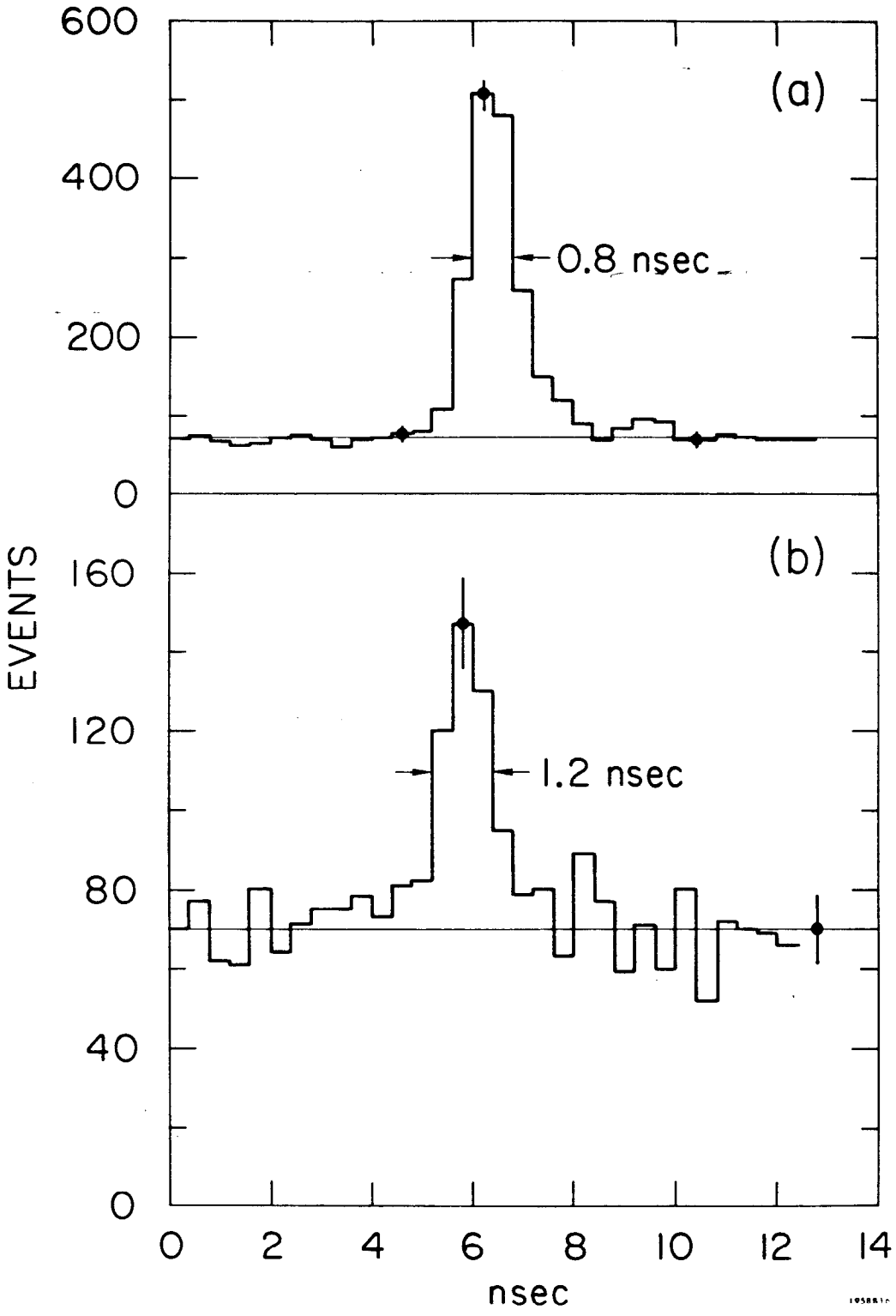

Fig. 1. Elimination of random background in ep → e'p'X using timing correlation. Plots (a) and (b) are two different kinematic settings.

where τ_o is the time for a particle travelling at the speed of light to traverse the same flight path (e.g. $\tau_o = d/c$ where d is the length of the flight path and c is the speed of flight.) Formula (1) has been used to produce the curves shown in Fig. 2 for various pairs of particles versus momentum. For these calculations a flight path of 1.5 meters was used ($t_o \simeq 5$ nsec) as this is a representative length for detectors used at storage rings.

The particle's mass is calculated using

$$M^2 = p^2\left(\frac{\tau^2}{\tau_o^2} - 1\right) \tag{2a}$$

and has an uncertainty of

$$\Delta M^2 = 2p^2\sqrt{\frac{M^2}{p^2} + 1}\left(\frac{\Delta\tau}{\tau_o}\right) \tag{2b}$$

due to the precision of the measurement of τ, $\Delta\tau$. Formula (2b) shows that particle identification using TOF measurements becomes worse as the square of the particle's momentum. To achieve the same mass resolution (and therefore the same level of particle identification) at twice the momentum requires a four-fold improvement in the TOF measurement ($\Delta\tau$ must be decreased by a factor of 4.)

To illustrate this technique, in Fig. 3 data from the Mark II collaboration are shown.[2] Clear bands of events occur at low momentum for π's, K's and P's. As the momentum is increased the bands broaden and eventually merge together at about 1 GeV/c. The TOF resolution for the counters used by the Mark II is quoted to be 300 psec for hadrons averaged over the entire system.

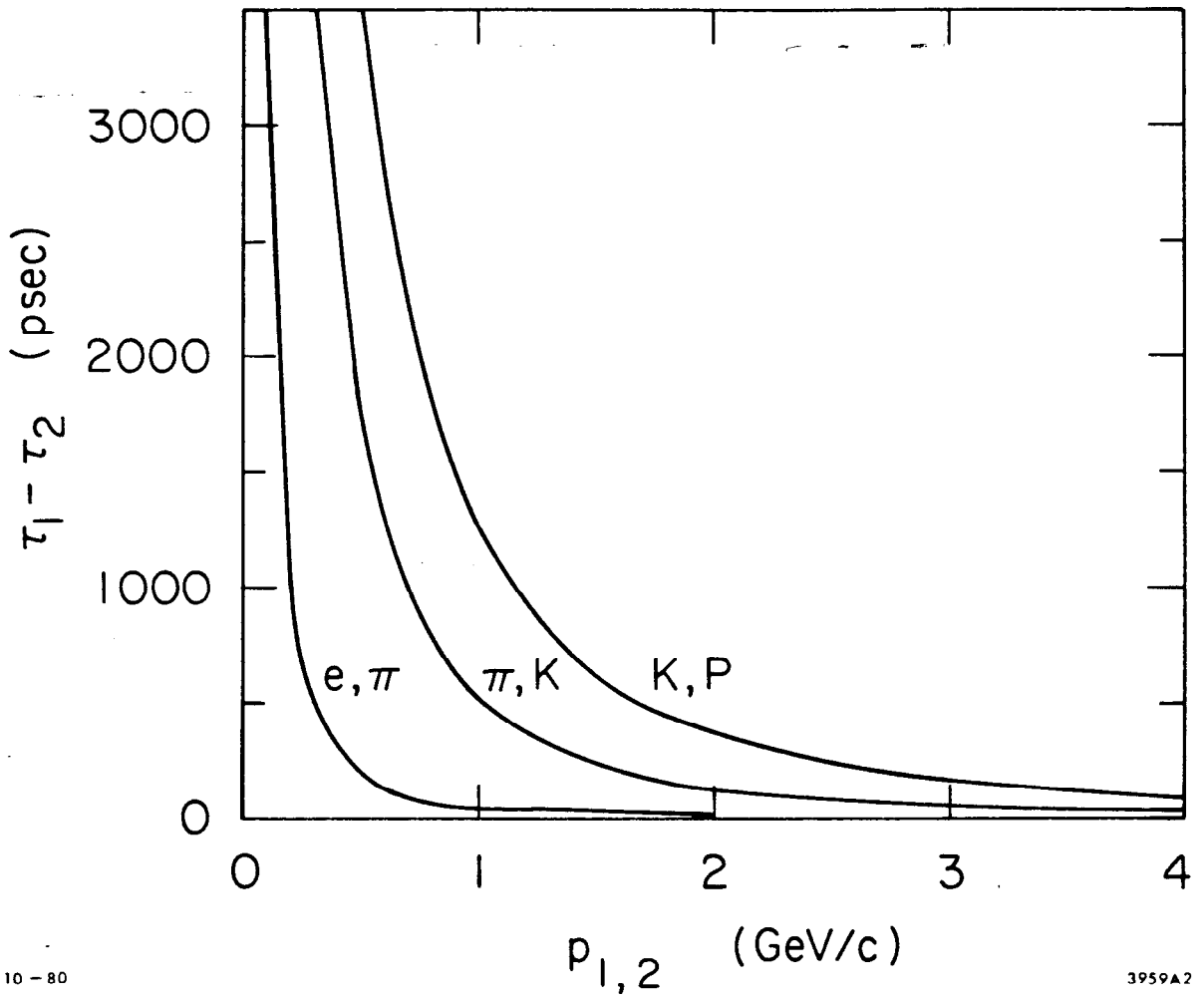

Fig. 2. Time-of-flight differences for various pairs of particles over a 1.5 m flight path versus momentum.

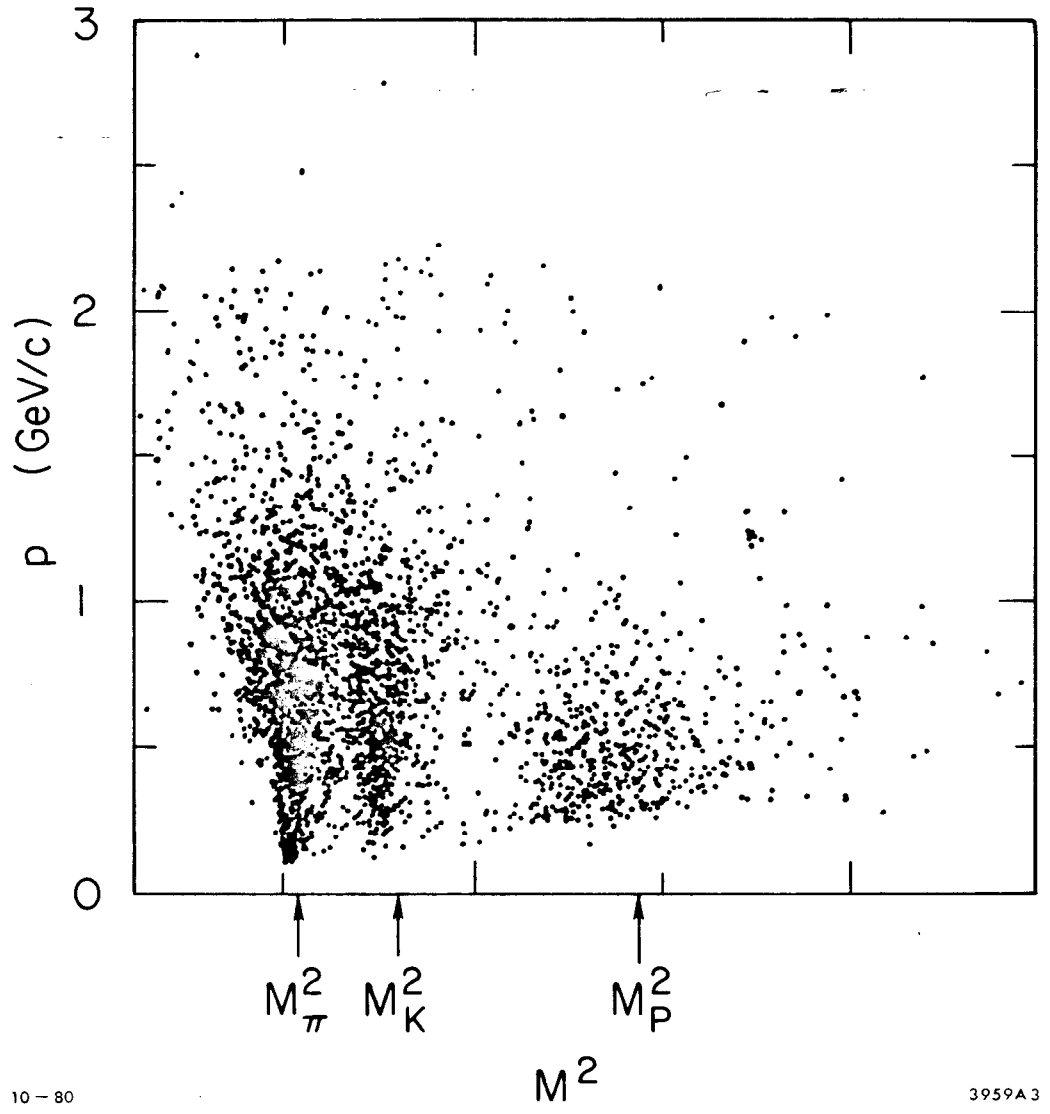

Fig. 3. Particle identification using time-of-flight and momentum measurements.

To place TOF measurements in perspective with other techniques for particle identification it is convenient to use the covarient velocity, $\eta(\equiv p/M)$. Using TOF measurements particles will be separable when

$$\eta \lesssim \sqrt{\frac{\tau_o}{2\Delta\tau}} \quad . \tag{3a}$$

Threshold Čerenkov counters will respond for

$$\eta \gtrsim \sqrt{\frac{1}{n^2 - 1}} \tag{3b}$$

where n is the index of refraction of the Čerenkov radiating medium. Energy deposition measurements (dE/dx) also scale in η and these three techniques for particle identification are shown in Fig. 4 versus η. Particles with η's to the right of the curve in Fig. 4a will be well identified. For threshold Cerenkov counters the range in momentum over which particles will be separated is $p_1 - p_2 = \eta(M_1 - M_2)$. For dE/dx measurements the range in momentum over which particles will be identified can be estimated by rescaling Fig. 4c by the appropriate particle masses; each particle type gives the same dE/dx curve shifted by an amount proportional to its mass. As such the curves for electrons, pions, kaons, and protons crossover each other in the momentum range of .8 GeV/c - 2 GeV/c.

π/K separation as a function of momentum and η is shown in Fig. 5 for these three techniques. This figure shows that the region where TOF measurements can play an important role is between 800 MeV/c and 2.0 GeV/c. This region is also covered by aerogel Čerenkov counters but the advantage of being able to distinguish backgrounds (such as cosmic rays) from events and achievable granularity of detectors makes TOF measurements the method of choice for most experiments.

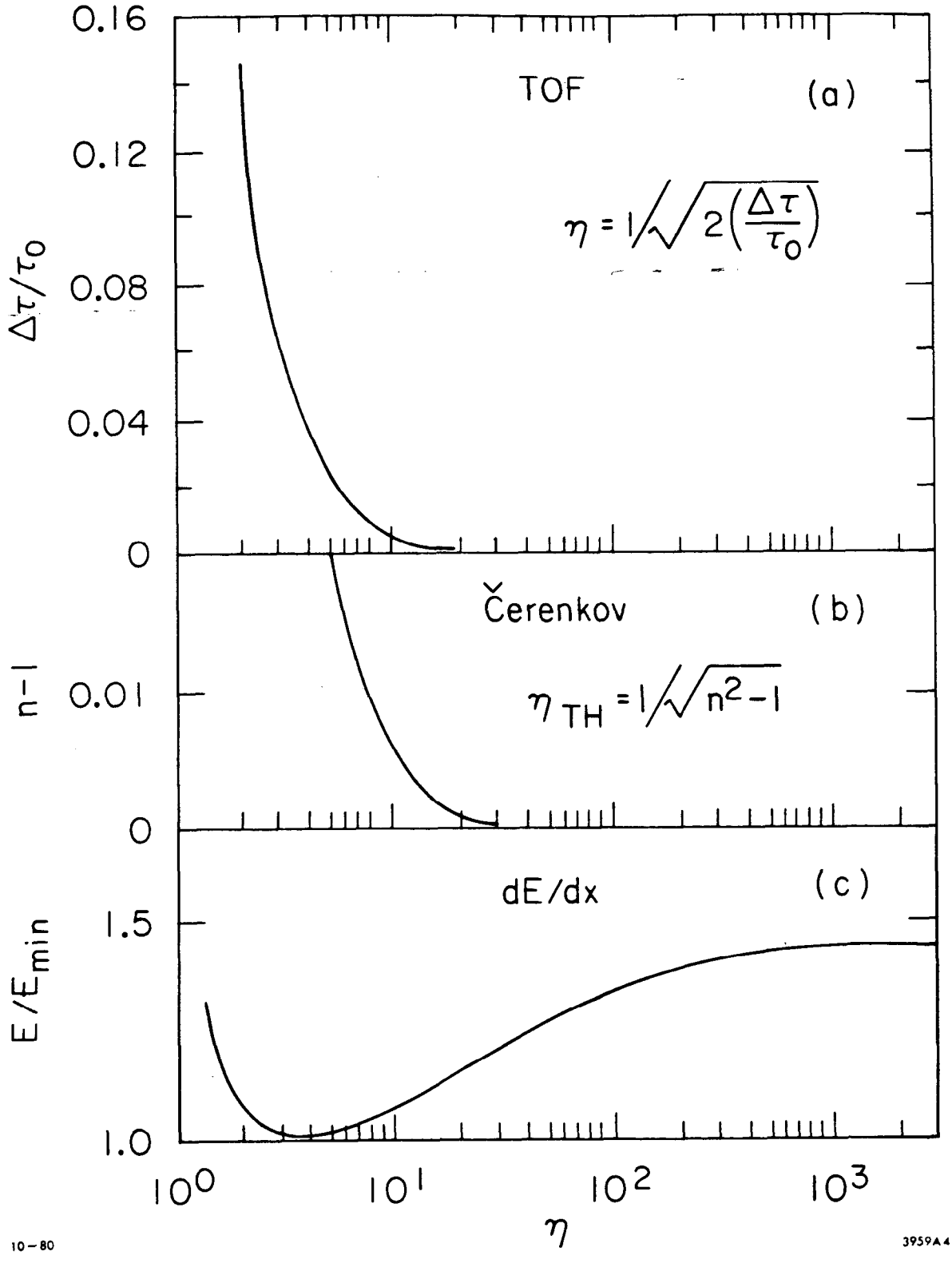

Fig. 4. Three techniques for particle identification:
(a) time-of-flight;
(b) threshold Čerenkov (n is the index of refraction); and
(c) dE/dx measurement.
The variable η is the covariant velocity $|\vec{p}|/M$.

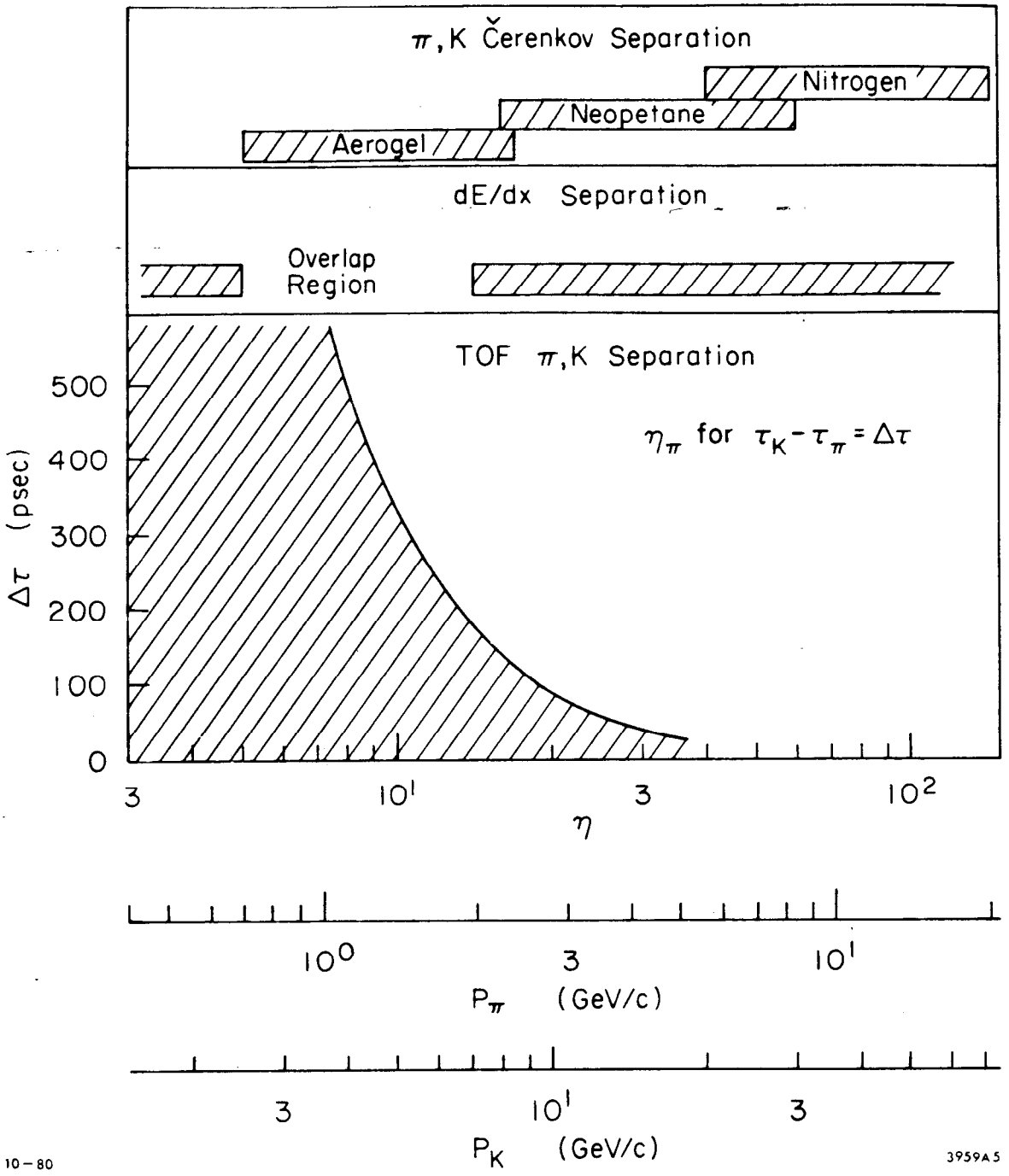

Fig. 5. π, K separation by 3 techniques.

In the following sections of these notes I will review two techniques for making TOF measurements: 1) conventional scintillation counters and 2) planar spark counters (PSC's).

II. SCINTILLATION COUNTERS

A typical scintillation counter is shown schematically in Fig. 6. The signals from each photomultiplier are pulse height analyzed. Its time of arrival is measured by first transforming it to a standard logic pulse in a discriminator and then using this pulse to stop a fast digital clock (TDC). If t_1 and t_2 are the respective signal arrival times from the discriminators connected to each end of the scintillator then the location along the scintillator where the particle penetrated the counter is given by

$$x = \left(\frac{t_1 - t_2}{2}\right) v_{eff} \quad . \tag{4a}$$

v_{eff} is the effective propagation velocity of light in the scintillator and $t_{1,2}$ are assumed to be corrected for additive constants arising from delay cables, the photomultiplier delay time, light pipe delay time, etc. The time of penetration is

$$\tau = \left(\frac{t_1 + t_2}{2}\right) - \frac{L}{2v_{eff}} \tag{4b}$$

where L is the length of the scintillator. From Eq. (4a) we see that x is independent of τ and similarly from (4b) that τ is independent of x.

Now let us consider what some of the sources for fluctuation in τ may be. The scintillator light results from energy deposited by particles that penetrate it. Approximately one photon is produced for every 100 electron volts of energy deposited. For plastic scintillator a

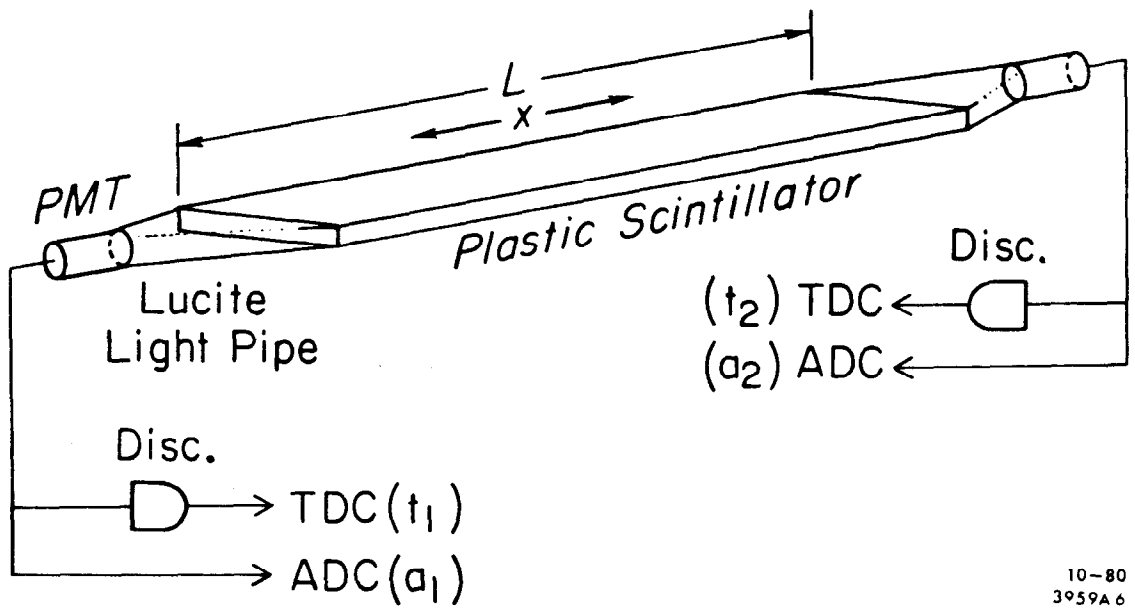

Fig. 6. Schematic diagram for a plastic scintillator, time-of-flight counter.

minimum of 2 MeV of energy is deposited per cm travelled for particles with unit charge which results in about 20,000 photons/cm being produced.

The time distribution for the light produced in three different types of scintillators is shown in Fig. 7 along with the time spectrum for Cerenkov light produced in lucite.[3] The latter is used to calibrate the response of the measuring apparatus.

The light pulses generated by the three scintillators shown in Fig. 7 are similar and a quantitative comparison is given in Table I.[3] Most groups building scintillator counter TOF systems have chosen NE110 or PILOT F. No significant difference in performance of these systems has been demonstrated.

After the light is produced it is transmitted to the photomultiplier via the scintillator plastic and a light pipe couples the round face of the phototube onto the usually rectangular scintillator cross-section. A calculation of the number of photoelectrons resulting from light that undergoes no bounces for typical counters (L = 300 cm × 2.5 cm thick) results in less than one. In fact much of the light bounces down the scintillator and light pipe at angles not much smaller than the total internal reflection angle. The "straight shot" light produced in the middle of the counter will require a time,

$$t_{min} = \frac{L}{2} \cdot \frac{n}{c} \tag{5a}$$

to reach the light pipe. In Eq. (5a) n is the index of refraction for the scintillator and is approximately equal to 1.58. If the maximum angle away from the "straight shot" direction that light can make is given by the total internal reflection angle, $\Theta_{INT} = \sin^{-1}\left(\frac{1}{n}\right)$, then the maximum time for light transmission is

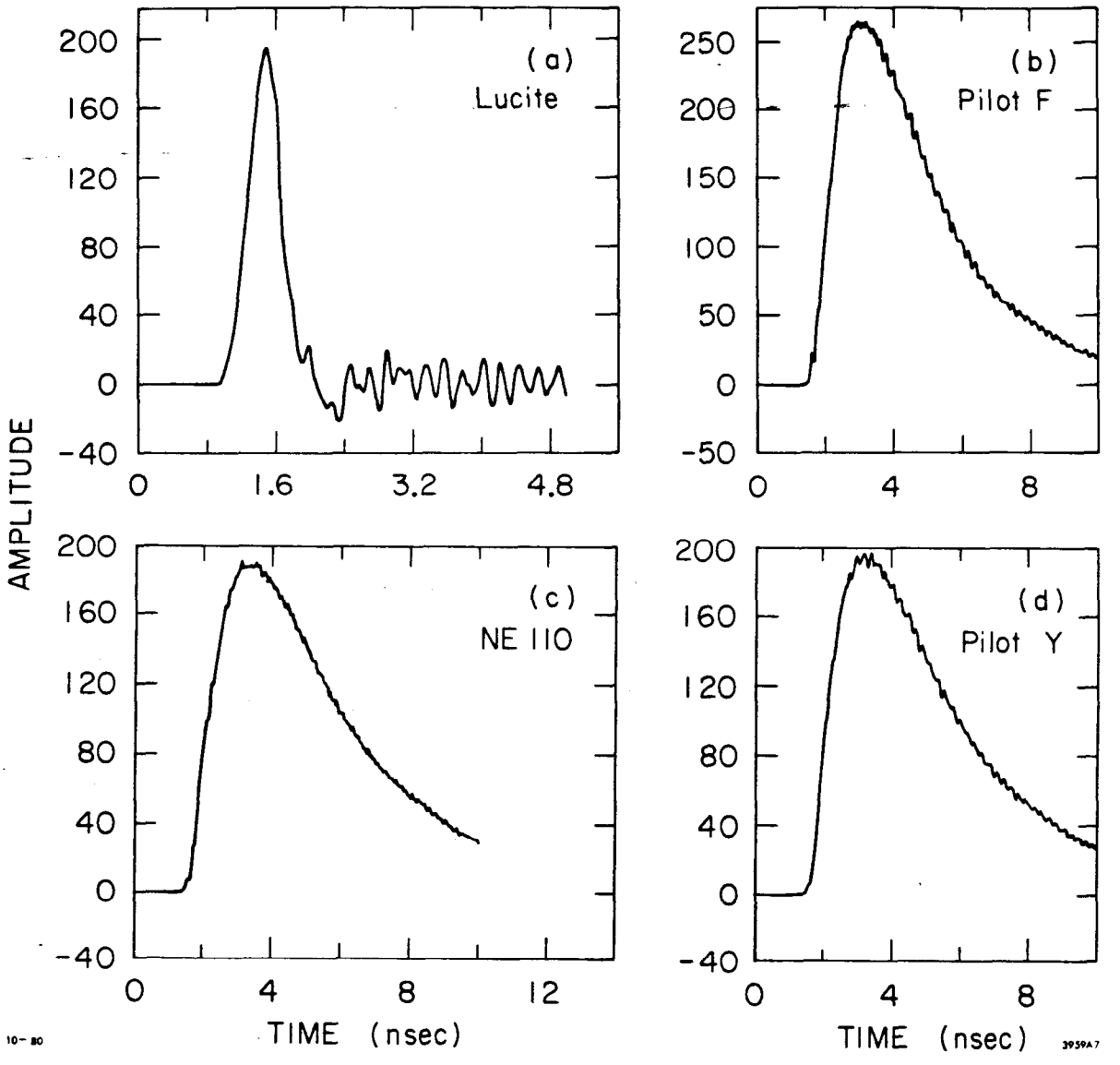

Fig. 7. Relative light output from various plastic scintillators. (a) shows the response of lucite used as a Čerenkov radiator for comparison.

TABLE I

Numerical evaluation of the plastic scintillators shown in Ref. 7.

Scintillator	Rel. Light Output	Rise Time (nsec)	Time for 10-90% Light Output (nsec)
Lucite	.05	.31	:51
PILOT F	1.00	.81	4.65
NE110	.88	.99	5.22
PILOT Y	.86	.88	5.13

$$t_{max} = \left(\frac{1}{\cos\Theta_{INT}}\right) t_{min} \simeq 1.3\ t_{min} \quad . \tag{5b}$$

Equations (5a) and (5b) show that the light emerges over a time interval approximately equal to .3 t_{min}. This time interval is proportional to the length of the scintillator, L. As such the density of photons per unit time decreases as 1/L.

The effective transit time for light in scintillator TOF counters is measured by plotting the time difference $\left(\frac{t_1 - t_2}{2} \text{ from Eq. (4a)}\right)$ versus the measured position of penetration for particles. The result is shown in Fig. 8.[4] The data have been fit to a straight line and the slope measures the effective velocity of light in the scintillator. v_{eff} is found by this technique to be 16.3 cm/nsec. This value for v_{eff} is also found by others.[2] From this value we can calculate the typical angle away from the "straight shot" direction by

$$\cos\Theta_{eff} = \frac{v_{eff}}{c/n} \simeq .84 \tag{6}$$

which gives $\Theta_{eff} \cong 33°$ (compare to $\Theta_{INT} \cong 39°$). In typical counters the light will have been internally reflected some 30 times before reaching the light pipe. This implies that the surface quality of the scintillator is very important.

The light pipe transmits the light emerging from the scintillator onto the photocathode. Usually the area of the photocathode is small compared to the cross-sectional area of the scintillator. Light will be lost in making this transition, but its important that these losses be minimized and uniform over the cross-section of the scintillator and that the transit time from all points on the end of the scintillator to the

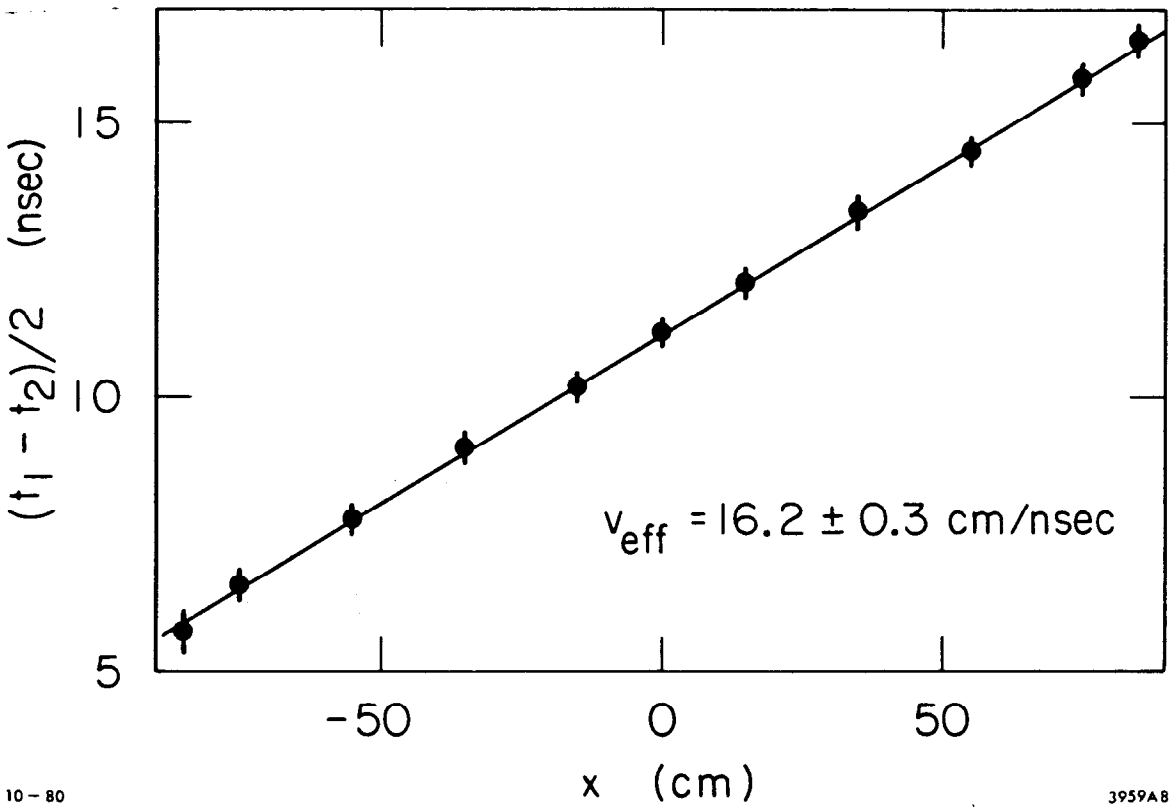

Fig. 8. Time difference versus position for a plastic scintillation counter.

photocathode be approximately equal. Monte Carlo computer programs are useful in modeling and optimizing the design of this piece of the system.[5]

The phototube produces the electrical signal that is measured by the electronics. Photons incident in the photocathode cause the emission of "photo-electrons" which are collected on the first of many dynode stages. These act as cascaded amplifiers. The time between light striking the photocathode to an output signal is about 30 nsec. Time jitter in phototubes comes about principally from different transit times of photoelectrons from different locations on the photocathode. These time differences have been measured to be about 190 psec for 2" tubes.[6] If a large number of photons strike the photocathode this jitter is reduced (for 100-photoelectrons the jitter is about 64 psec). To minimize this effect care should be used in designing the base for the phototube. The focussing elements between the photocathode and the first dynode have a significant effect on the time jitter. The voltage drop between the photocathode - first dynode is also important and a change of one part in a thousand can change the delay time by 20 psec. Some experimenters choose to stabilize this voltage drop by using zener diodes.[4]

The signals coming from the phototubes are processed by fast electronics producing a time of arrival and a measurement of the integrated charge in the pulse. Other schemes have been used, but this one is the most common and simplest to describe. It has been observed that the time of arrival is correlated with the pulse height. The principal correlation is sometimes modelled[4] to be

$$\tau = t - W\left(\frac{1}{\sqrt{a_o}} - \frac{1}{\sqrt{a}}\right) - \frac{x}{v_{eff}} \qquad (7)$$

where τ is the corrected time, t is the measured time minus any constant effects, W is a fitted parameter, a_o is a reference pulse height, a is the measured pulse height and x/v_{eff} is the position correction due to the delay time for light to travel down the scintillator. An example of $\frac{1}{\sqrt{a}}$ versus t is shown in Fig. 9.[4] The line in Fig. 9 indicates the fit for the parameter W.

Another method was proposed by M. Wollstadt[7] in which the dV/dt of the leading edge of the phototube pulse is measured. This is accomplished by using two discriminators with different threshold voltages, each connected to fast a TDC. The corrected time is then calculated by linearly extrapolating to V = 0. The impressively good results of Wollstadt using this method has not been successfully applied universally. Some report good success while others report no improvement.

We have now reviewed the major aspects of scintillation counter TOF systems and will now compare the results achieved by various groups. The discussion about how the light emerges from the scintillator indicated that the density of photo-electrons per unit time would be proportional to (N_e/L) where N_e is the average number of photo-electrons and L is the counter's length. I conjecture that the time resolution will be proportional to $(1/\sqrt{N_e/L})$ if the contribution from the phototube and electronics is negligible. The data for nine different counters is given in Table II. The time resolutions quoted are for particles crossing near the center of the counters and have been fully corrected for amplitude and position effects. In Fig. 10 these best time resolutions are plotted against $\sqrt{L/N_e}$. The straight line in Fig. 10 indicates the following "rule-of-thumb":

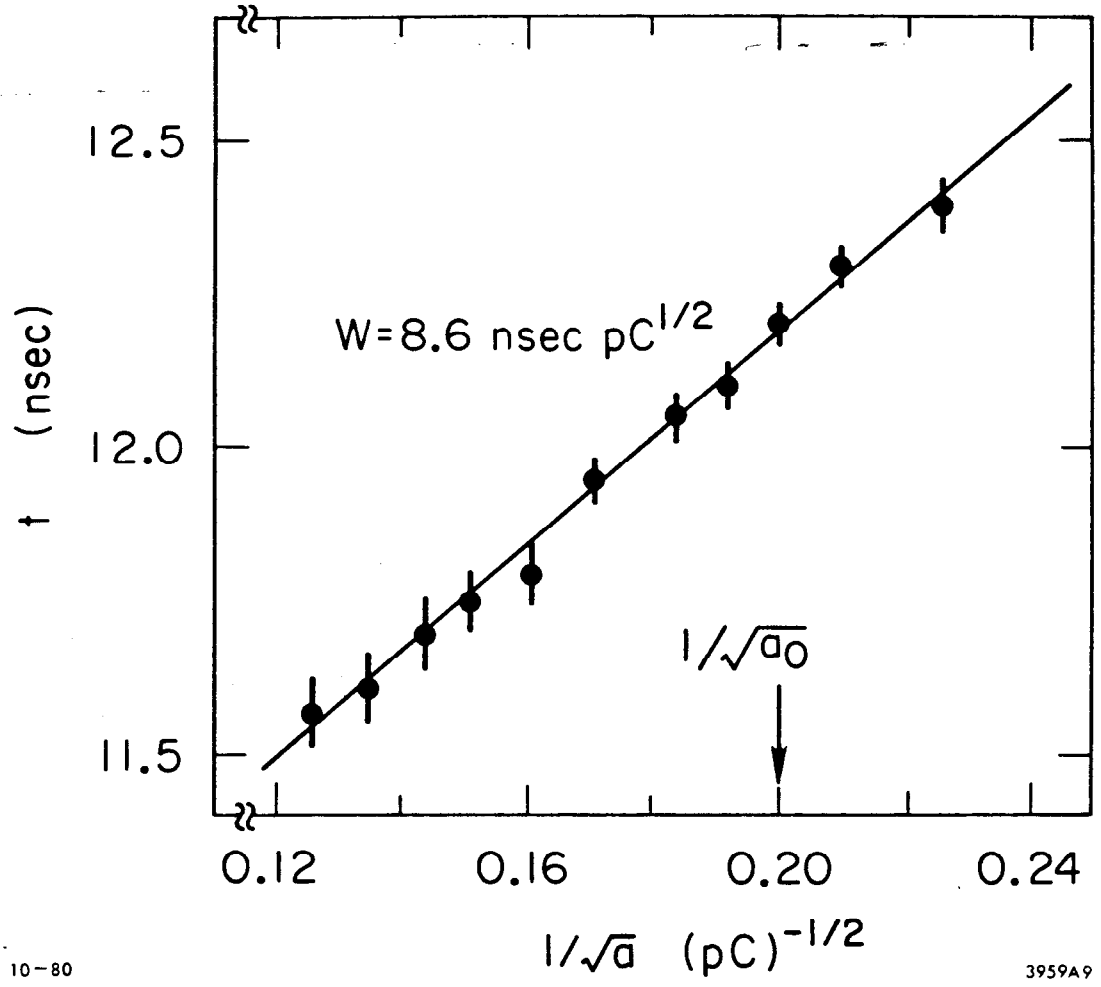

Fig. 9. Time correlation with pulse height a. a_0 is a reference pulse height.

TABLE II

Comparison of nine time-of-flight counters. L is the counter length and N_e is the average number of photoelectrons for minimum ionizing particles. Photoelectron yields which are stared (*) are my estimates based on the thickness of the scintillators. This was done when this information was unavailable from the references.

Counter	L(cm)	N_e	$\Delta\tau$(psec)
1) MARK II[2]	350	40	255
2) "Free Quark Search" (PEP-14)	315	90	166
3) DASP[4]	172	28*	212
4) F. Binon et al., N.I.M., 153, 409 (1978)	25	28*	92
5) M. Wollstadt[7]	100	39*	144
6) M. Wollstadt[7]	50	16*	152
7) MARK III[5]	300	120	140
8) M. Wollstadt[7]	100	260*	85
9) Same as 4)	~.2	4500*	48

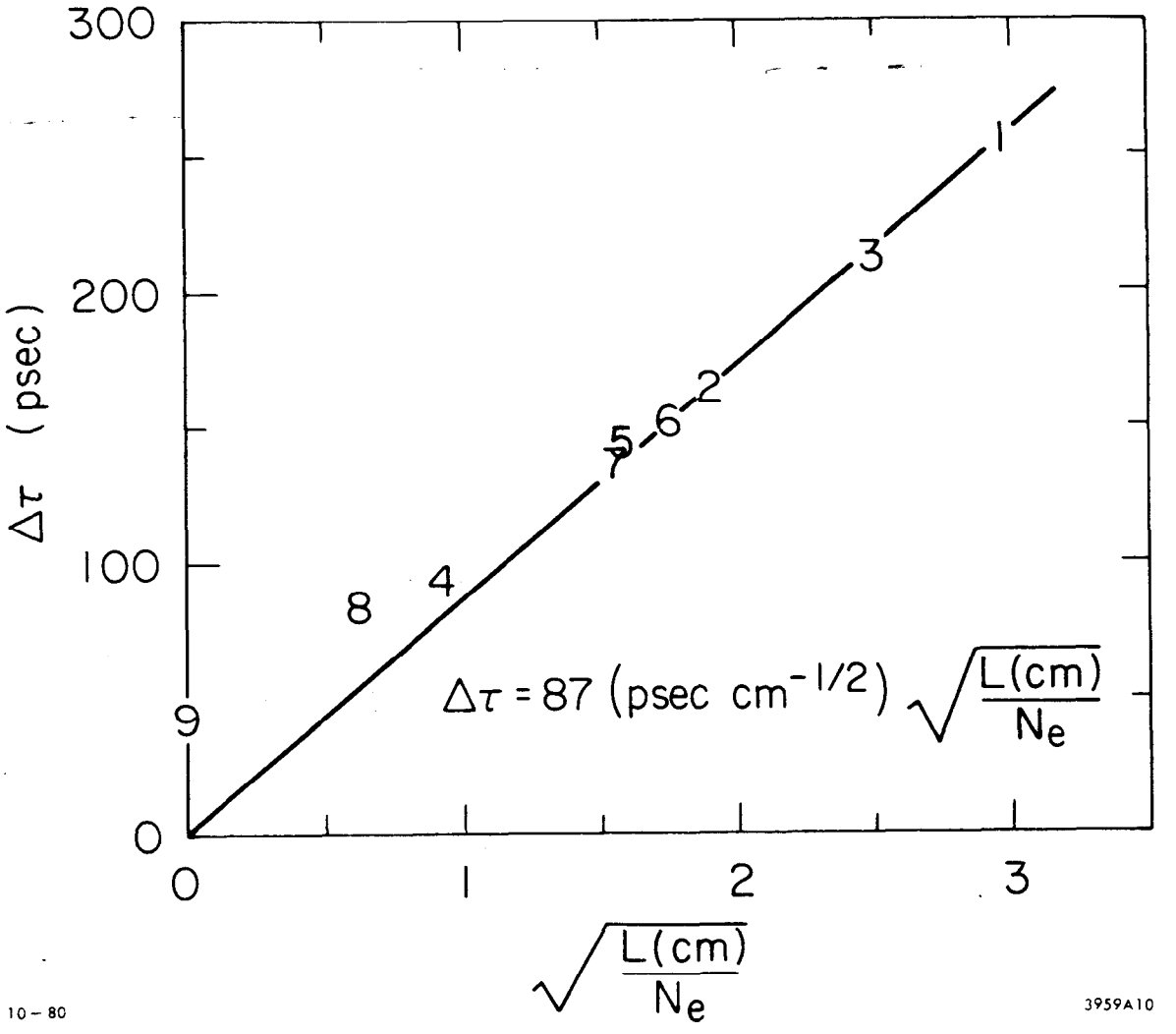

Fig. 10. A comparison of the time-of-flight counters listed in Table II. L is the length of the counter and N_e is the average photo-electron yield for minimum ionizing particles.

$$\Delta\tau = 87(\text{psec-cm}^{-\frac{1}{2}})\sqrt{\frac{L(\text{cm})}{N_e}} \quad . \tag{8}$$

Results from counters with expected resolutions $\gtrsim$ 100 psec agree well with Eq. (8). Below the 100 psec level other effects such as the photo-tube jitter certainly will contribute and will dominate the time resolution.

I have glossed over many important points and hope this will serve as an introduction to scintillation TOF systems. I have not described the necessary calibration procedures for large systems. Experimenters designing and constructing TOF systems are referred to the references I have given and should talk to these authors directly. The details of how they accomplished the results given in Table II are important.

III. PLANAR SPARK COUNTERS

Planar spark counters (PSC's) are considerably older particle detectors than plastic scintillators. J. Keuffel at CALTECH is usually given credit for their invention in 1949.[8] I will not describe the history of the development of these counters and refer interested people to the references. A major advance was the introduction of high resistance semi-conducting glass for one of the electrode surfaces. This glass sufficiently limits the discharges to minimize damage to the electrode surface.

A PSC is shown schematically in Fig. 11. The anode is made of semi-conducting glass with a volume resistance of 10^9 - 10^{10} Ω-cm.[9] Typical anodes used in test counters have had an area 9 cm × 9 cm to 30 cm × 30 cm and were 5 to 8 mm thick. The large flat surfaces are ground flat and polished. All corners and edges are

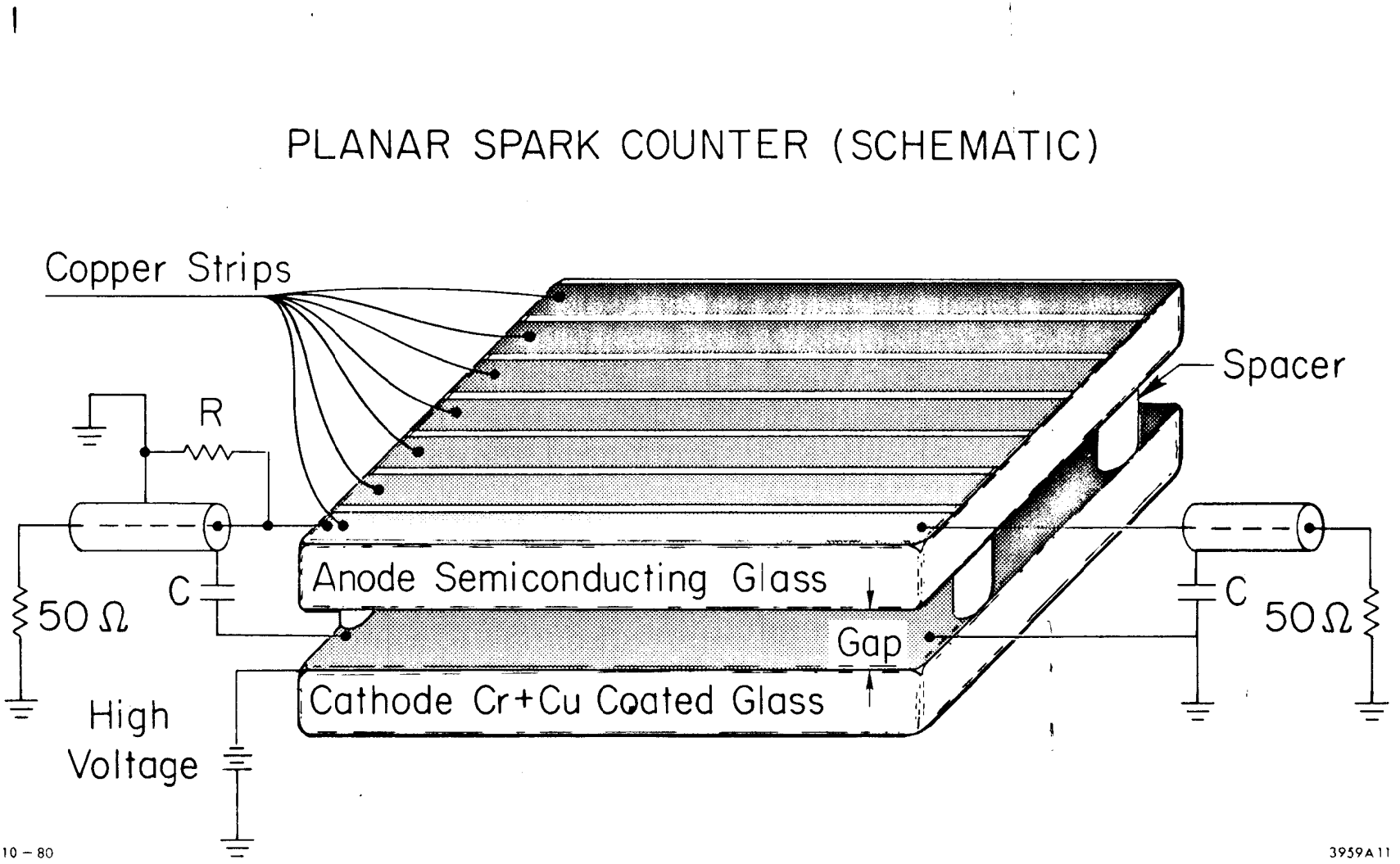

Fig. 11. Schematic diagram of a Planar Spark Counter (PSC).

rounded and polished. Copper strips are deposited over a thin layer of chrome on the surface opposite the electrode surface. The chrome is deposited first as it sticks well to glass; copper doesn't. The copper strips form one half of a transmission line that conducts the high frequency signals caused by sparks in the gap to the ends of the counter. The surface over which the strips are deposited should be polished to minimize the attenuation of high frequencies. The thickness of the copper should be $\gtrsim 5$ μm, a thickness which is several times the skin depth for the high frequency signals.

The cathode can be made from ordinary float cast, window glass. As with the anodes, edges and corners are rounded and polished. The electrode surface is formed by depositing a thin layer of chrome followed by a thick layer of copper. The deposition process is repeated with polishing and washing occurring before each Cr-Cu deposition. Typically 2-3 layers of copper are put on in this manner. The thickness of the copper is again $\gtrsim 5$ μm as this surface forms the other half of the transmission lines.

The two electrode surfaces are held apart to form a gap of 100-200 μm. The gap should be uniform to a few percent. To accomplish this two techniques have been used so far. The first, used by the experimenters at Novosibirsk[10] consists of "outriggers" placed well away from the gap. The second, used by us at SLAC, are metallic shims placed inside the gap between the semi-conducting anode and copper cathode. This short circuits the gap at the spacer's location and the semi-conducting glass limits the current to <1 μA. The semi-conducting glass also grades the electric field from zero at the spacer to full value in a distance

proportional to the thickness of the semi-conducting glass. The "outrigger" and "in-gap-spacer" schemes result in dead area and a more clever approach needs to be found.

Between the electrodes, gas at high pressure (6-10 Atmos) is circulated. Its composition is argon with 10% - 30% organic gases added to quench u.v. light. A typical gas mixture is 2% 1,3 butadiene, 2% ethylene, 10% isobutane (or propane), 5% hydrogen, and the balance is argon.

The strip lines are coupled to coaxial cables at each end of the counter. The anode side is connected directly to the center conductor and the cathode side, via a high voltage blocking capacitor, to the cable shield. A capacitor of a few hundred pico-farads is sufficient and is usually incorporated as a parallel plate capacitor with the copper cathode surface forming one half of the capacitator.

The sequence of events in a PSC which results in a spark begins with the counter in its quiescent state. The electric field strength, E, in the gap is large: $3\text{-}5 \times 10^5$ V/cm. Typical values of E/P (P is the gas pressure) range from 40-70 V/cm-torr. When a particle passes through the counter it creates N_o primary ion pairs. For the counters being described here N_o is in the range of 4-8 and is proportional to $P\delta$ where δ is the gap dimension. These initial ionizations quickly avalanche and this process can be described as a function of time, t, by

$$N(t) = N_o \, e^{\alpha v t} \tag{9}$$

where α is the number of ion pairs produced per unit length of drift for electrons (α is the first Townsend coefficient) and v is the electron drift velocity. The value $1/\alpha v$ is the time required for the avalanche

to grow by "e" and sets the time scale for these counters. "Fast" counters have large values of αv. The length for an avalanche to grow by "e" is $1/\alpha$ and is typically 1-2 μm for the operating conditions I am describing.

A streamer develops when space charge effects become important in the developing avalanche. This is called Meek's criterion[11] and occurs when there are $\sim 10^8$ electrons present in the avalanche. The streamer quickly propagates to both electrode surfaces, bridging the gap with a column of ionized gas. The subsequent spark depletes the surface charge on the electrodes. This causes the electric field in the region of the spark to fall almost to zero. The organic gases absorb u.v. photons produced in the discharge in a distance away from the spark which is short compared to the distance required for recovery of the electric field. The organic gases are crucial in ensuring the containment of the discharge to a small region about the spark. When the surface charges on the semi-conducting glass have been neutralized by the discharge, current ceases to flow. Gradually, the surface charges are reestablished on the semi-conducting glass. During this time the slower positive ions are gently swept from the gap. After a few milli-seconds the electric field is restored. During this process only that region of the counter in the vicinity of the spark is "out-of-action." The rest of the counter remains "live."

I will now discuss some of the operating characteristics of PSC's. Figure 12 shows the measured counting rate in a PSC with a gap of 185 μm, an area of 100 cm^2 and 6 atmospheres pressure.[10] This figure shows the non-coincident, or "singles" rate and the rate on the plateau part of the curve is consistent with the calculated cosmic ray rate

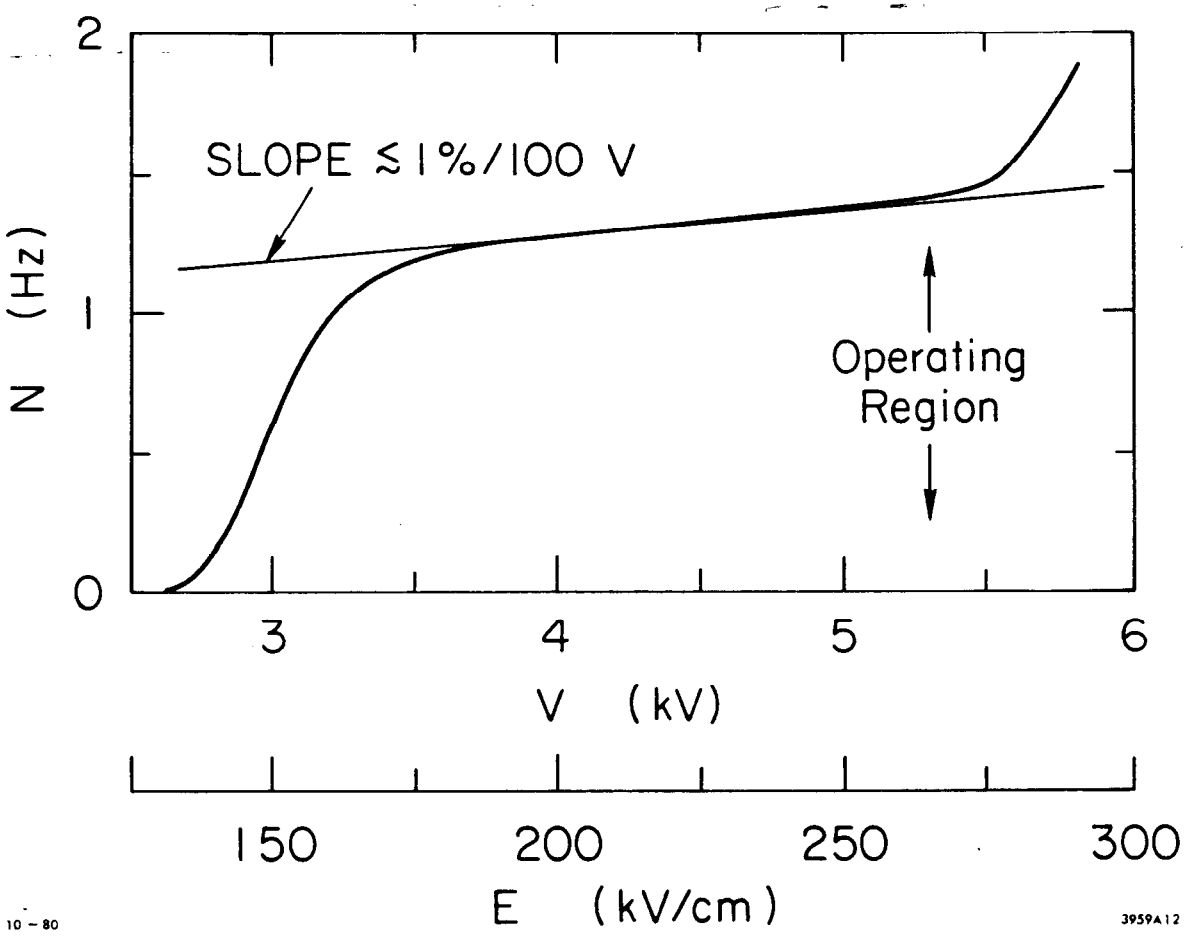

Fig. 12. Plateau curve for a PSC with a gap dimension of 185 μm and run at 6 atmos pressure. N is the singles counting rate and V is the voltage across the spark gap.

through the counter. In good counters the plateau extends to approximately twice the voltage at which signals are first observed and is very flat with a slope not exceeding 1%/100 volts.

The threshold voltage is determined by the gas pressure and composition and the gap dimension δ. If the distance an avalanche requires to form a streamer is Z_c, then at threshold $\delta = Z_c$. Only those electrons produced at the cathode surface will develop sufficient space charge, N_s, to induce a spark. The threshold curve can then be formulated as

$$\eta = 1 - e^{-N_o(1 - \frac{Z_c}{\delta})} \tag{10a}$$

where η is the probability for the counter to spark due to the passage of a charged particle and Z_c is calculated using

$$N_s = e^{\alpha Z_c} . \tag{10b}$$

The usual model for the first Townsend coefficient α is

$$\alpha = APe^{-BP/E} . \tag{10c}$$

The threshold portion of the plateau can then be fit to determine the parameters A and B in Eq. (10c). Typical values for these parameters are A = 6 cm^{-1} $torr^{-1}$ and B = 110 V/cm-torr.[10] I will use the value of B later on to estimate the time resolution attainable in PSC's.

The slow rise in the plateau curve is presumably noise which at low voltage is at a very low level but eventually increases abruptly at high voltage near the end of the plateau curve. In order to obtain the best time resolution from PSC's one operates as close to the end of the plateau curve as possible.

The output pulse shape for PSC's seems to be controlled by the high frequency characteristics of the counter. The final growth of the spark is very rapid and the subsequent current flow excites signals on the strip transmission lines. The signals propagate in both directions along the strip lines to the ends of the counter. The rise time of the leading edge of the subsequent output pulse is probably limited by the high frequency cut off of the strip lines themselves. We have measured the rise time for typical PSC's and find it to be ~300 psec for a 9 cm long strip line. The pulses are about 5 nsec wide and have an amplitude of several volts at the highest operating voltages. The pulse height distribution near threshold is very narrow and the sparks are probably being localized and quenched by the large resistivity of the semi-conducting glass. At the highest operating voltages the pulse height distribution has a much larger mean value and is about 100% FWHM. A typical pulse height distribution is shown in Fig. 13 at high voltage.

The maximum voltage obtainable for a fixed operating pressure depends on the u.v. light absorption properties of the gas. Ultraviolet photons must be absorbed by the gas before travelling far enough through the gap to regions of high electric field where a secondary spark may be induced through photo-ionization. The various organic gases mentioned earlier were selected to extend the u.v. absorption of the gas to long wavelengths. In particular the 1-3 butadiene and ethylene extend the absorption of u.v. light from 1600 Å (the isobutane cut off) to about 2250 Å. The u.v. absorption properties of these gases is shown in Fig. 14 (Ref. 12).

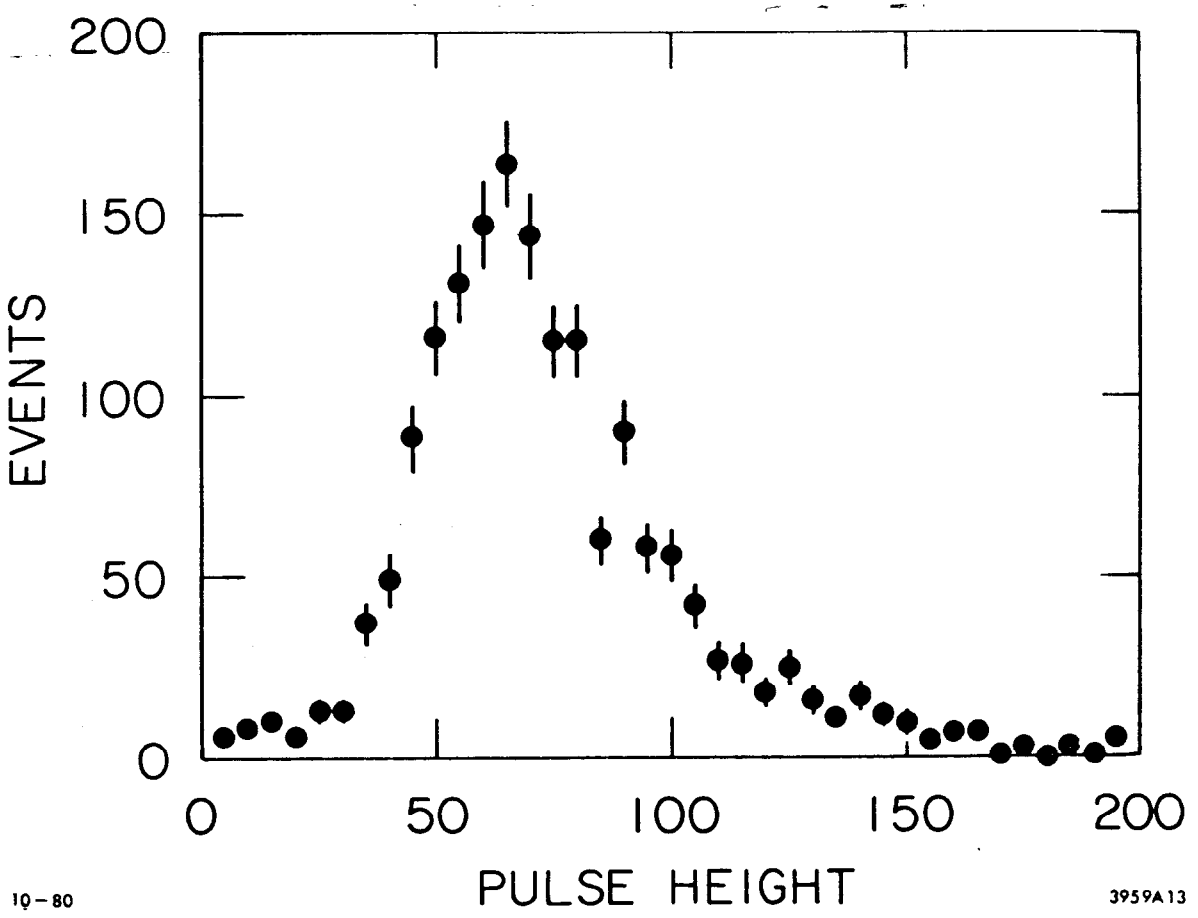

Fig. 13. Pulse height distribution for a PSC with a gap dimension of 180 μm run at 10 atmos, and 6800 volts.

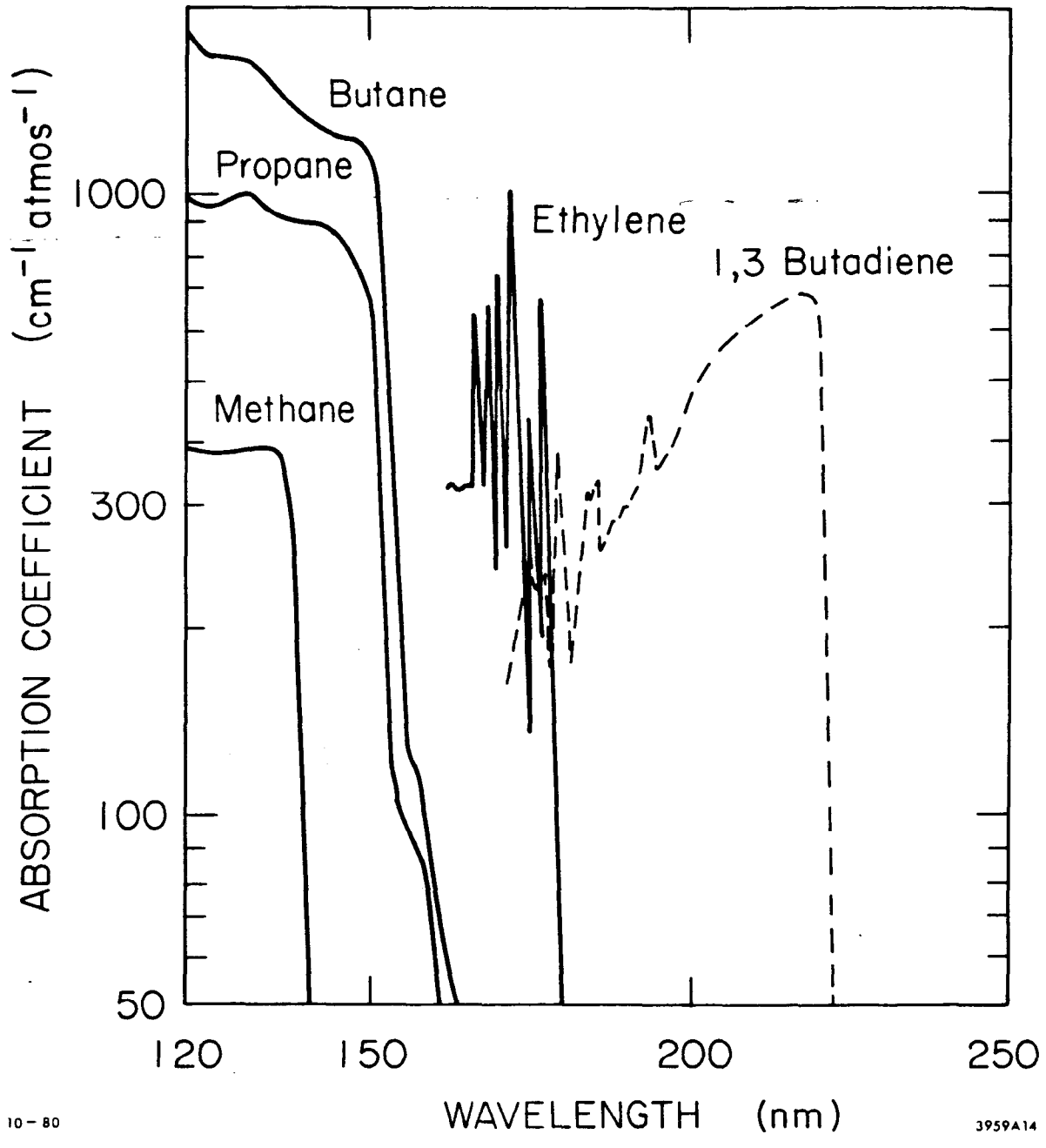

Fig. 14. u.v. light absorption coefficients for various organic gases used in PSC's.

The amount of charge in each spark has been measured by two techniques. The first is to integrate the charge in the signals from the strip lines.[10] The second method is to measure the total current drawn by the counter as a function of counting rate. The rate of increase in current with counting rate is interpreted as the charge per count. Both methods show that sparks at the higher operating points have a few nanocoulombs of charge.

The charge measurement can be used to estimate the size of the sparks, r_s. This is done by equating the spark's charge, Q_s, to an area times the surface charge density, σ_s:

$$r_s = \sqrt{\frac{Q_s}{\pi\sigma_s}} = \sqrt{\frac{Q_s}{\pi\varepsilon_o E}} \quad . \tag{11}$$

E is the electric field strength at the electrode surface

$\varepsilon_o = 8.85 \times 10^{-14}$ farads/cm. Substituting numbers into Eq. (11) results in $r_s \simeq 1.3$ mm. In Ref. 10 a different calculation indicated a value for r_s of about 3 mm.

In any case the sparks are small, as they must be in order to minimize damage to the electrode surfaces. What is of real interest is not the spark size, but the size of the insensitive area about the location of a spark. In the counters constructed at SLAC, as mentioned earlier, the gap is "shorted" out by metal spacers at four locations. For semi-conducting glass thickness of 5 mm a "dropping-off" of the pulse height is observed for distances closer to the spacer than about 5 mm. In Ref. 10 the authors report calculated values of .35 cm^2 for the insensitive area. Our measurement for the insensitive area about the spacers is about .75 cm^2. As our measurement is around a D.C. short, it is probably an overestimate of the dead area caused by sparks.

The recovery time for the field in the gap after a spark has occurred is controlled by the resistance and thickness of the semiconducting glass. For the counters constructed at SLAC we calculate the recovery time to be about 10 msec. The recovery time should be kept long compared to the time necessary to sweep the positive ions left in the wake of a spark from the gap. This time is a few milliseconds.[10]

The delay time, t_D, after the passage of a charged particle through the spark gap until a streamer is formed is proportional to $\frac{1}{\alpha v}$. Variations in t_D can come from many sources but it is hard to imagine sources that don't also scale as $\frac{1}{\alpha v}$. In Ref. 10 measurements of both t_D and the time resolution are presented and a graph of these measurements is shown in Fig. 15. The ratio of t_D to the time resolution is approximately constant and both change very rapidly with increasing electric field strength.

An analytic model for $\frac{1}{\alpha v}$ can be formed by using Eq. (10) for α and the following model for v:

$$v = k\left(\frac{E}{p}\right) \quad . \tag{12}$$

k is a constant which depends on the gas. Thus

$$\frac{1}{\alpha v} \propto \frac{1}{E} e^{BP/E} \tag{13}$$

The lines in Fig. 15 indicate the variation in $\frac{1}{\alpha v}$ using the value of B determined from the fit to the threshold curve.

In Table III data for three different counters are given.[8,10] If B is assumed not to be strongly dependent on the composition of the gas then a comparison of these counters is possible by introducing a correction for the various E/P values at which measurements were made. These

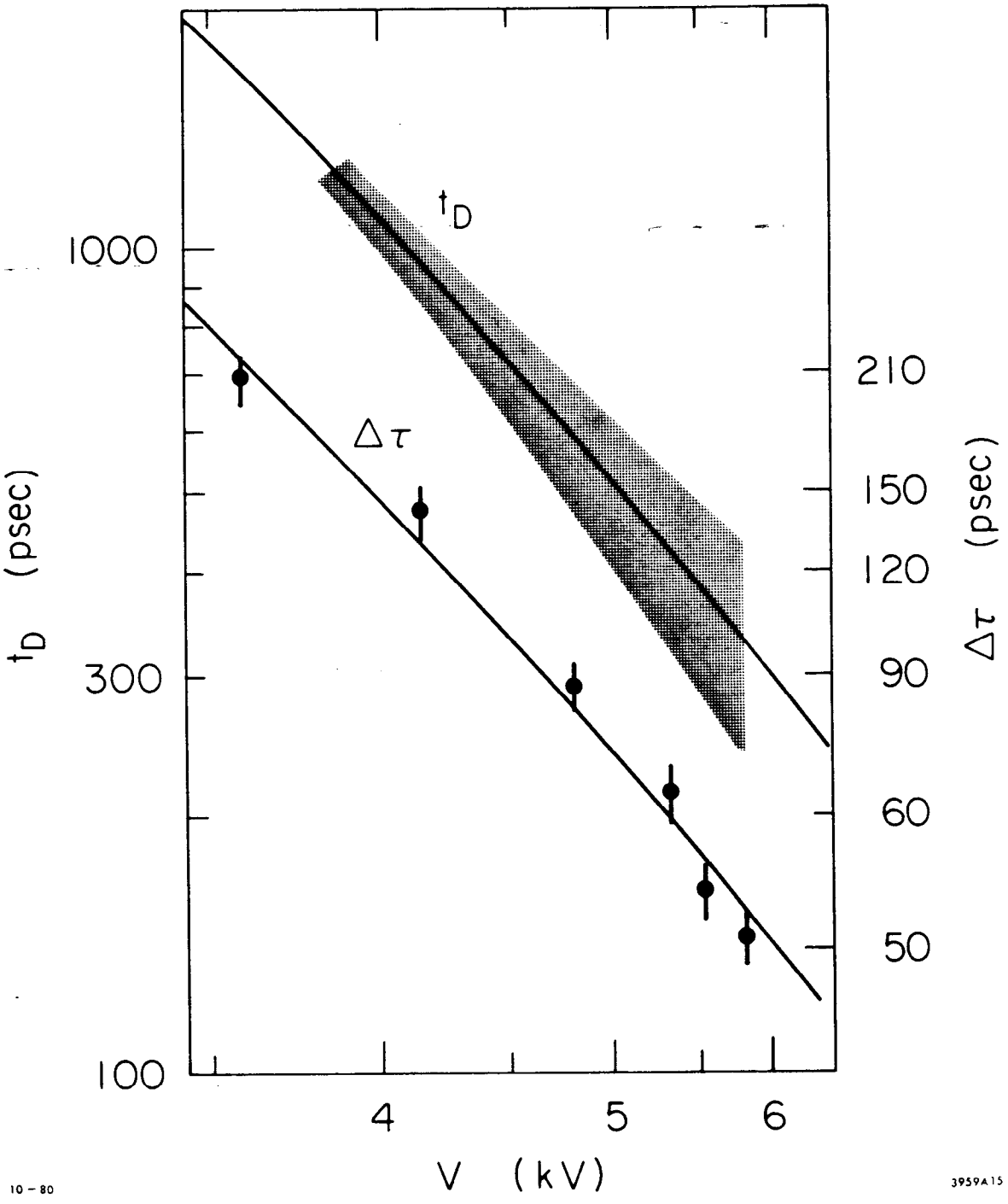

Fig. 15. The delay time between the passage of a particle thru a PSC and the spark and the RMS time resolution of the same PSC versus the gap voltage V. The shade area around t_D indicates the size of the measurement errors.

TABLE III

Operating properties of three PSC's. $\Delta\tau_{corr}$ is the time resolution corrected to E/P = 70 V/cm-torr using $\Delta\tau_{corr} = \Delta\tau \exp\left[B\left(\frac{1}{70} - \frac{P}{E}\right)\right]$. I used 110 V/(cm-torr) for B.

Reference	GAP(cm)	P(torr)	V(volts)	N_0	E(V/cm)	E/P(V/cm-torr)	τ(psec)	τ_{corr}(psec)
Ref. 8e	.10	755	5500	3.3	5.5×10^4	72.9	285	303.0
Ref. 10a-c	.0185	4530	5800	3.6	3.14×10^5	69.2	47	46.2
	.0185	4530	5500	3.6	2.97×10^5	65.6	51	45.9
	.0185	4530	5350	3.6	2.89×10^5	63.8	63	54.1
	.0185	4530	4850	3.6	2.62×10^5	57.9	88	63.4
	.0185	4530	4150	3.6	2.24×10^5	49.5	144	75.1
	.0185	4530	3580	3.6	1.94×10^5	42.7	210	76.9
Ref. 10d	.010	9060	6000	3.6	6×10^5	66.2	28	25.6

corrected values (to E/P = 70 V/cm-torr) given in column 8 of Table III and are plotted against E in Fig. 16. A fit to these data gives the following "rule-of-thumb" for the time resolution of PSC's:

$$\Delta\tau(\text{psec}) \simeq \frac{4.7 \times 10^6}{E^{1.03}_{(\text{volts/cm})}} \; e^{110 \frac{P(\text{torr})}{E(\text{V/cm})}} \qquad (14)$$

One should note that N_o is approximately the same for all of the counters shown in Table III and so any dependence on N_o would not be revealed. It may in fact turn out that a major source of time fluctuations in PSC is controlled by the number of primary ion pairs and hence result in an overall $\sqrt{\frac{1}{N_o}}$ dependence. No good experimental evidence is yet available to confirm or debunk this conjecture.

The time resolution for a pair of 9 cm × 9 cm counters constructed at SLAC is shown in Fig. 17. These data were collected using a cosmic ray telescope equipped with drift chambers for particle tracking. Shown in Fig. 17 is the difference in the end-to-end time averages from the strip lines for the two counters. Both counters were run at P = 12 atmos. and had 185 μm gaps. The high voltage was 6800 volts in one counter and 7500 volts in the other.

A PSC can also provide a position measurement in much the same way as conventional scintillation TOF's do. This is done by taking the difference of the times measured at each end of the strip lines and correlating this with the measured location of the particle crossing. Using the drift chamber information from the cosmic ray telescope we can fit straight line trajectories for the particle tracks. The results of the difference from the fitted track location in the PSC to that predicted using the time difference (à la Eq. (4a) where v_{eff} is replaced with

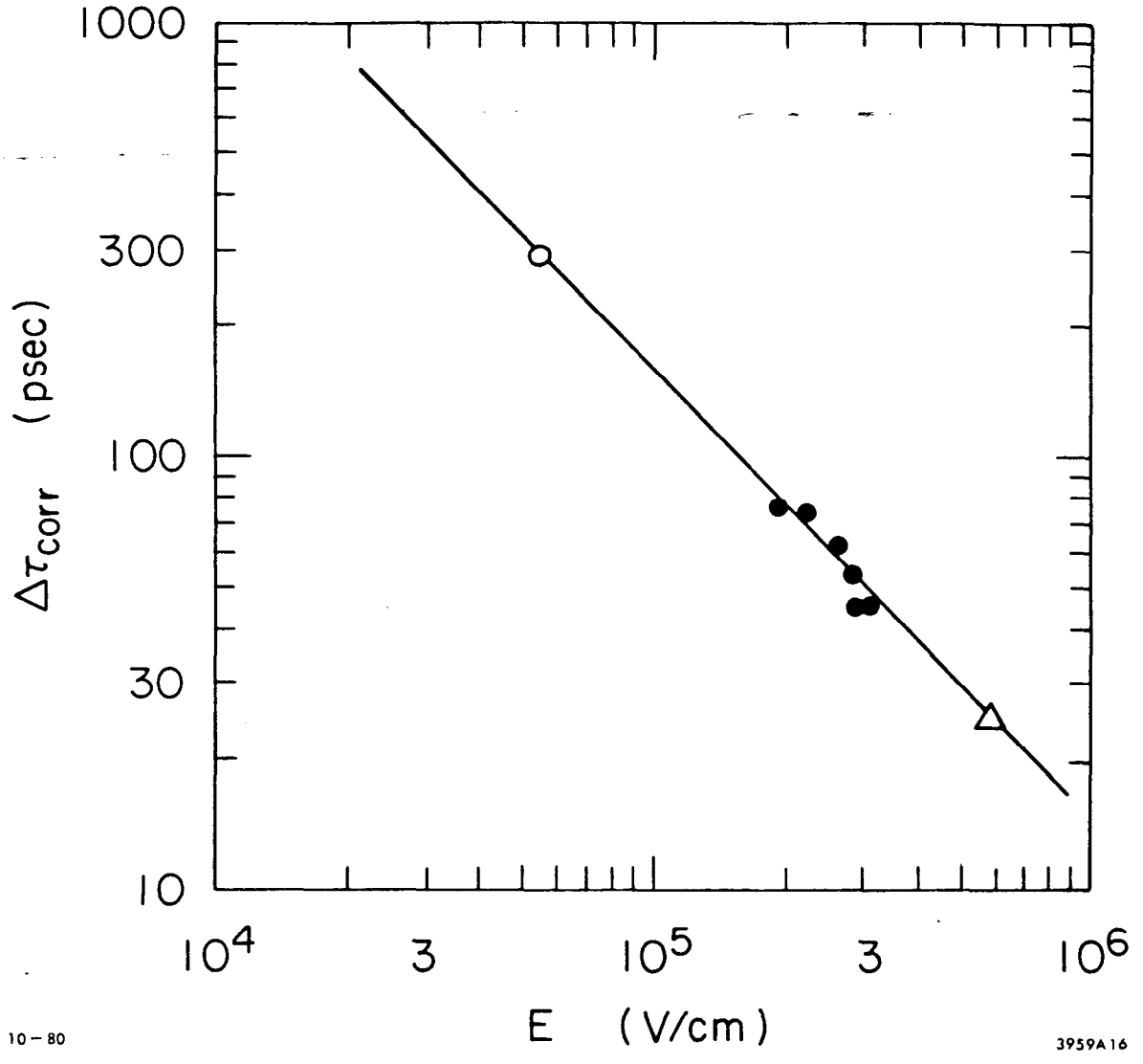

Fig. 16. Three PSC's run with different gaps and pressures: (o) 1000 μm gap, 1 atmos, (●) 185 μm gap, 6 atmos, and (Δ) 100 μm gap, 10 atmos.

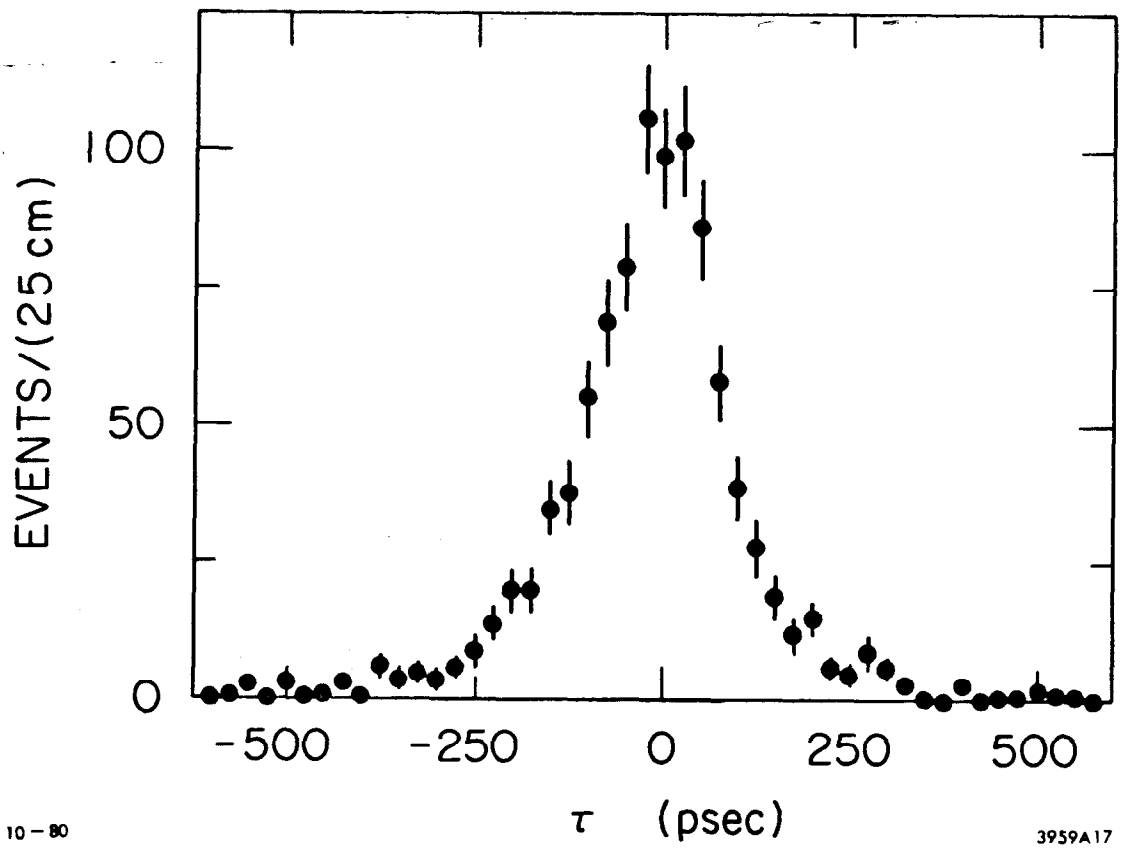

Fig. 17. Time difference spectrum from a pair of PSC's with 180 μm gaps run at 12 atmos. RMS resolution for a single counter is 55 psec. Data taken with cosmic rays.

the speed of signals in the strip lines: $v_{signal} \approx 15$ cm/nsec) is shown in Fig. 18.

The position accuracy in PSC's should not be correlated with the timing accuracy. This is because the timing accuracy is controlled by fluctuations in the delay time t_D. The same spark is the source for the signals at both ends and insofar as the spark occurs on a very fast time scale, the position resolution just reflects the timing accuracy of the electronics used to make the measurements. The measured position resolution of 2.4 mm can thus be interpreted as a time resolution of the electronics of about 16 psec RMS which is to be compared with the expected RMS of 14.4 psec arising from the 50 psec bin size in the TDC units used.

I have tried to explain what PSC's are and have glossed over many important points with respect to their construction. I will mention two before concluding this section. These counters are difficult to make and require a high standard of cleanliness not usually present in the workshops where particle detectors are constructed. The standards used in the manufacture of integrated circuits are closer to what must be achieved. The second point is that an extended "burning-in" period is required for PSC's. This is accomplished using an intense radioactive source to make the counter spark $\sim 10^5$ times per square centimeter. During the burn-in period the high voltage is slowly increased with attention to the singles rates which should be kept below about .04 Hz/cm^2. It has been conjectured[10] that during this initial period of use, a film of polymerized gas coats the electrode surfaces, covering up small imperfections that would otherwise lead to spontaneous breakdown.

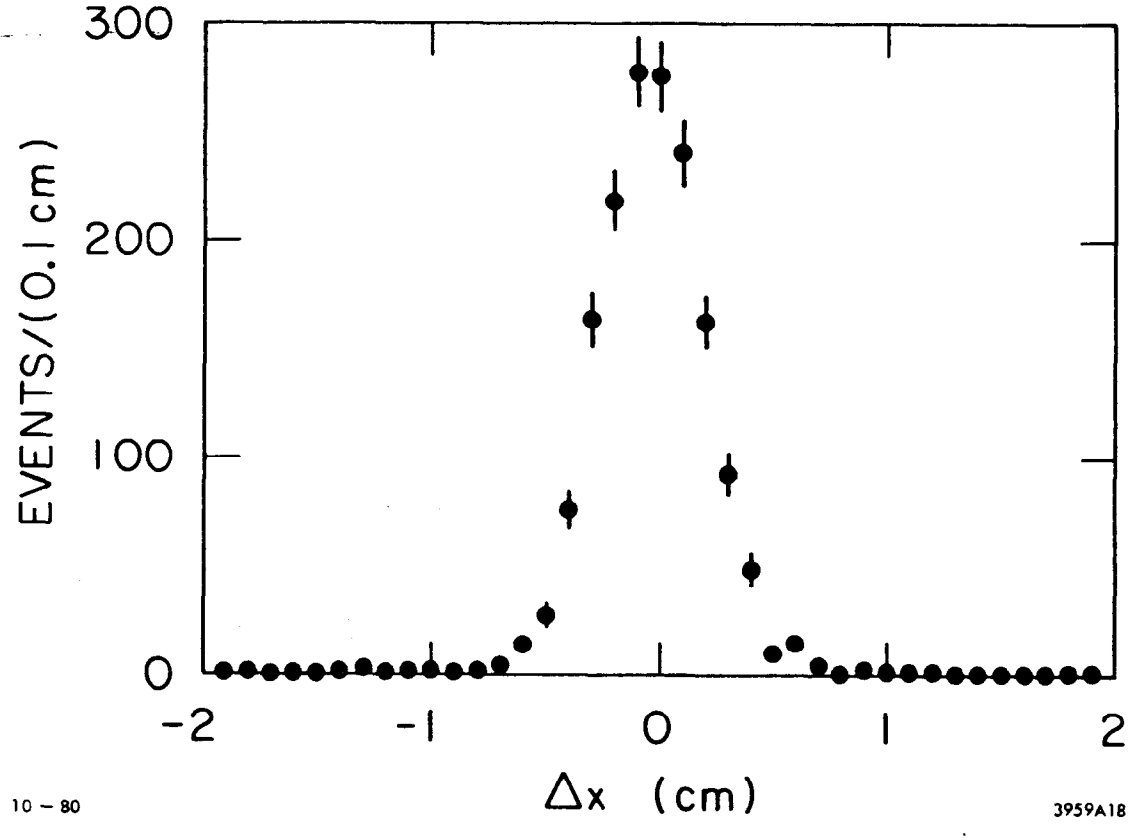

Fig. 18. Position determination in a PSC infered from the difference in times measured on each strip. The location of particle penetrations was determined by reconstructing straight line trajectories from drift chambers.

No information yet exists on the maximum lifetime of PSC's. Greater than 10^7 sparks/cm^2 seem to not adversely affect the counter's performance. Whether or not PSC's can withstand the sometimes severe radiation environments present at storage rings is also unknown.

We are presently constructing 20 cm long PSC's here at SLAC and will then make 120 cm long counters. Our 9 cm × 9 cm counters have performed adequately enough to encourage us that these large counters can be made to work well with time resolutions at or below the 50 psec level.

Referring back to the introduction where particle identification using TOF was discussed, optimistically we might expect to be able to separate the various particle types using PSC's to momenta above 3 GeV. This would nicely complement the dE/dx technique using drift chambers by providing particle identifications in the "cross-over" region. The good position resolution along the strip lines in PSC's and the possible number of strip lines (limited by the number of TDC channels) could be made to result in a small number of ambiguous TOF measurements.

ACKNOWLEDGEMENTS

I gratefully acknowledge many useful discussions with Jeff Weiss of the Mark II collaboration and Dave Dorfan of Santa Cruz. I thank Art Ogawa for carefully reading this manuscript. I also wish to acknowledge the collaboration with Yuri Pestov from Novosibirsk during 1978 which made possible the construction of PSC's at SLAC.

REFERENCES

1. E. D. Bloom et al., SLAC-PUB-955 (1971).

2. J. Weiss (private communication).

3. J. Kadyk and M. Alam, MARK II Internal Note, Sept. 29, 1976.

4. W. Braunschweig et al., N.I.M. 134, 261-266 (1976).

5. D. Dorfan (private communication).

6. Branko Leskovar et al., IEEE Trans. on Nuc. Sci., Vol. NS-25, No. 1, 582 (1978).

7. Michael Wollstadt, BONN-IR-76-39, Universität Bonn (1976).

8. a) J. Keuffel, Rev. of Sci. Inst. 20, 202 (1949).
   b) F. Bellu and C. Franzinetti, Nuovo Cimento, X, No. 10, 1461 (1953).
   c) M. V. Babykin et al., Soviet Jour. of Atomic Energy, VI, 487-494, (1956).
   d) E. K. Zavoisky et al., Soviet Jour. of Atomic Energy, VI, 495-499 (1956).
   e) V. Parkhomchuck et al., N.I.M. 93, 269-270 (1970).

9. We have used semi-conducting glass made by U.S. Schott Optical in Dureay, Penn., glass type S8900. Alternate semi-conducting glass types are available from German Schott Optical.

10. a) V. D. Laptev et al., UDC 539.1.074.27, 1698 (1975).
    b) V. D. Laptev et al., UDC 539.1.074.27, 1703.
    c) A. D. Afanas et al., UDC 539.1.074.27, 1701.
    d) Yu. N. Pegtov et al., SLAC translation 184 (1978).

11. L. B. Loeb and J. M. Meek, The Theory of the Electric Spark, Stanford University Press, Stanford, California, Chapter II (1941).

12. H. Siebke, Diplomarbeit in Physik (in German), Aachen (1980).